

Visualization of geometric influences on proximity effects in heterogeneous superconductor thin films

Jungdae Kim, Victor Chua, Gregory A. Fiete, Hyoungdo Nam, Allan H. MacDonald and Chih-Kang Shih*

The proximity effect is a central feature of superconducting junctions that plays a key role in many devices and can be exploited in the design of new systems with quantum functionality^{1–12}. Recently, exotic proximity effects have been observed in various systems, including superconductor–metallic nanowires^{5–7} and graphene–superconductor structures⁴. However, it is still not clear how superconducting order propagates spatially in a heterogeneous superconductor system. Here we report on intriguing junction geometry effects in a heterogeneous system consisting of electronically two-dimensional superconducting islands on a metallic substrate. Depending on the local geometry, the superconducting gap induced at the metallic surface sometimes decays within ~ 20 nm of the superconductor, and sometimes survives at distances that are several coherence lengths from a superconductor. We show in particular that the curvature of the junction plays an essential role in the proximity effect.

The sample system comprises superconducting two-dimensional (2D) Pb islands on top of a single-atomic-layer surface metal, the striped incommensurate (SIC) phase of the Pb overlayer on Si(111) (refs 13–16). The scanning tunnelling microscopy (STM) image shown in Fig. 1 captures a variety of junction configurations. Figure 1a shows an interesting ‘ π ’-shaped Pb island five monolayers (ML) thick on top of the SIC surface. Previous scanning tunnelling spectroscopy (STS) studies have shown that the SIC phase is superconducting with $T_{C,SIC} = \sim 1.8$ K (ref. 17) and the 2D Pb islands have a T_C around 6 K (ref. 18), although the actual T_C value also depends on the lateral size as well as its thickness¹⁹. At 4.3 K, the SIC template is in the normal state. At locations far from the Pb islands, the tunnelling spectrum exhibits no gap (spectrum no. 2 in Fig. 1b), whereas the spectrum acquired at the 2D Pb island shows a clear superconducting gap (spectrum no. 3). In the SIC region near the 2D Pb island, a superconducting gap can also be observed (spectrum no. 1), indicative of a proximity effect. To address the spatial dependence, we performed spectroscopic mapping over the same area, whose differential conductance at zero bias (zero-bias conductance (ZBC)) is shown in Fig. 1c. As the ZBC directly correlates with the size of the tunnelling gap (the smaller the value of ZBC, the larger the tunnelling gap), the landscape of ZBC is a good representation of the landscape of the superconducting gap.

The ZBC image reveals a rich landscape. In some regions (for example, region α), the induced superconducting gap decays very quickly within a very short distance from the SIC/superconductor (S) interface, whereas in region β where the SIC wetting layer is surrounded by Pb islands from both sides, the induced

superconducting gap is quite uniform. Similarly, in region γ where the SIC region is near the ‘recess’ of the Pb island, the induced superconducting gap propagates quite extensively. Figure 1d illustrates the spatial dependence of the tunnelling spectra along the arrow (starting at position (1) and ending at point (2), as shown in Fig. 1a), exhibiting a deep and uniform superconducting gap in the channel region that then decays quickly beyond the region marked by the dashed line.

These diverse superconductor configurations are investigated further according to the local junction geometry. Figure 2 shows the case for a simple S–Normal metal (N) junction with the normal metal region being the SIC template. The STM image and corresponding ZBC image are shown in Fig. 2a and b, respectively. The short-ranged proximity effect at the SIC surface near the junction interface is clearly evident from the ZBC image and this can be confirmed in the colour-scale plot of dI/dV in Fig. 2c taken along the dashed line in Fig. 2a. Shown in Fig. 2d are the line profiles of ZBC across the junction and the profile of the superconducting gap along the same line (Δ versus x). Note that the ZBC scale is upside-down to be consistent with the strength of the gap. The gap value is obtained by fitting the normalized dI/dV spectra with the Bardeen–Cooper–Schrieffer (BCS) density of state (DOS; examples shown in inset)²⁰. More detailed descriptions of the gap value deduction can be found in refs 18 and 19. A simple exponential fit of ZBC versus x yields a proximity length of 12 nm. However, a more sophisticated theoretical simulation yields a proximity length of 22 nm (see Supplementary Information and the accompanying Supplementary Fig. S5). We have studied many simple S–SIC junctions and found a consistent behaviour. In all cases, the induced gap decays very quickly from the interface with a proximity length of 20 ± 5 nm. In addition, the gap value in isolated Pb islands is always very uniform (to within 5%). Nevertheless, a hint of very small decay (<5%) can be identified occasionally (as shown in Fig. 2d). Except for the fact that Δ is very uniform up to the very edge of Pb islands, this observation is qualitatively consistent with a phenomenological description²¹, as summarized in Fig. 2e. In this picture, the decay length in the metal, ξ_M , is predominantly a property of the metal in proximity contact with S, ξ_S is the effective superconducting coherence length and b is the extrapolation length, which depends on the nature of the junction. In our case, ξ_M is about 20 nm whereas b is very large (in the limit of $b \rightarrow \infty$, the Δ in S would be a constant). ξ_M depends on the mean free path of the SIC surface metal, which inevitably contains crystallographic defects. A large b value may be a result of the fact that most of the S island edge interfaces with the vacuum and the S–SIC interface

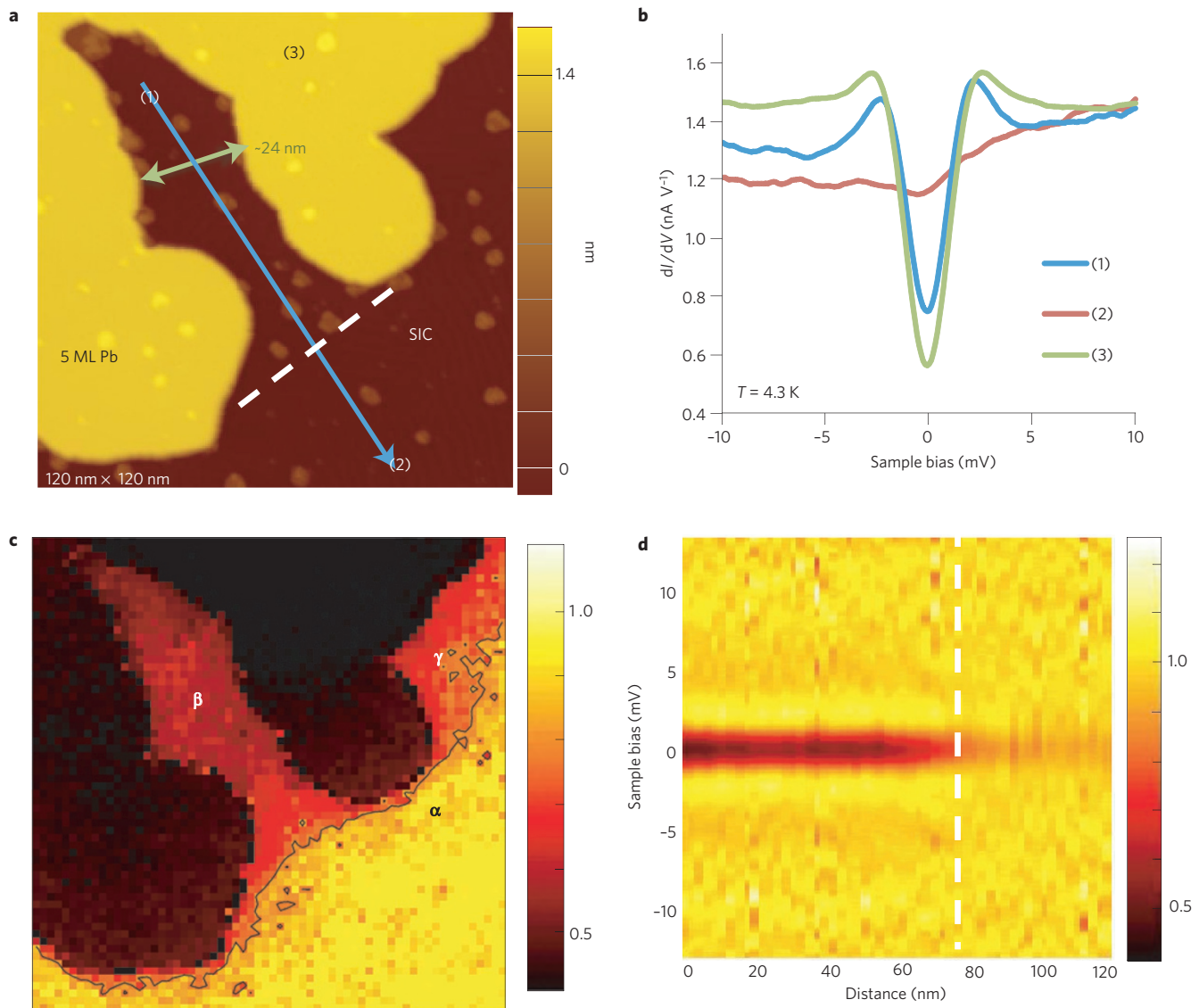


Figure 1 | Visualizing superconducting-gap landscapes in heterogeneous superconductor islands. **a**, STM topography image of a 'π'-shaped Pb island sitting on top of a SIC surface (sample bias $V_s = 0.3 V$, tunnelling current $I_t = 10 pA$). **b**, Differential conductance spectra at 4.3 K measured from the different locations labelled in **a**. **c**, Normalized ZBC image measured at 4.3 K for the same area of **a** that shows the marked transition of induced superconducting gap on SIC surface between inside and outside of 'π' shape as the colour contrast reflects the variation of local superconductivity. Also shown is a constant ZBC contour at a ZBC value of 0.78 (corresponding to a small superconducting gap value). **d**, The spatial dependence of superconducting gap spectra at 4.3 K measured along the arrow in **a**. The white dashed line represents the border of confined geometry in **a**.

exists only along the bottom edge, which is a line contact single atom thick. The simple S–S heterojunction follows the conventional picture where the order parameter changes continuously across the interface with a characteristic length scale of about 25 nm on either side of the junction (Fig. 2f). Interestingly, this characteristic length scale turns out to be very similar to the coherence length deduced from magnetic susceptibility measurements on Ge-capped thin Pb films²².

These conventional behaviours of proximity effects at a simple single-sided S–N or S–S junction change markedly in a more complicated junction geometry. Figure 3a shows two separated Pb islands with the SIC layer in between, creating a variety of junction geometries. For example, along arrows 1 and 2 are S–N–S heterojunctions with different widths of SIC (N) in between. Also marked with arrow 3 is a simple S–N junction. We map out the induced superconducting gap as a function of distance in the SIC regions along these three arrows using STS. The resulting

Δ versus x profiles at two different temperatures are plotted in Fig. 3b. Also shown in Fig. 3c,d are the colour-scale representation of the dI/dV maps along the two S–N–S double junctions. The spatial mapping of spectra along arrow (1) revealed a surprisingly uniform and well-developed superconducting gap, in contrast to a quick decay of induced gap being observed for the simple S–N junction of arrow (3) (refer to Fig. 2c). Similarly, along arrow (2) the induced gap is also relatively uniform, albeit with a smaller gap value than that along arrow (1). Most surprisingly, this relatively uniform gap value extends over a length scale that is about two times the characteristic decay length, indicating that the S–N–S junction is fundamentally different from the one-sided S–N junction. We observe this persistent proximity effect in all S–N–S double junctions with widths of up to 90 nm (see Supplementary Information). Considering that the Pb island and the SIC wetting layer is connected only through a line contact of one atom thick, this extended proximity effect is quite surprising.

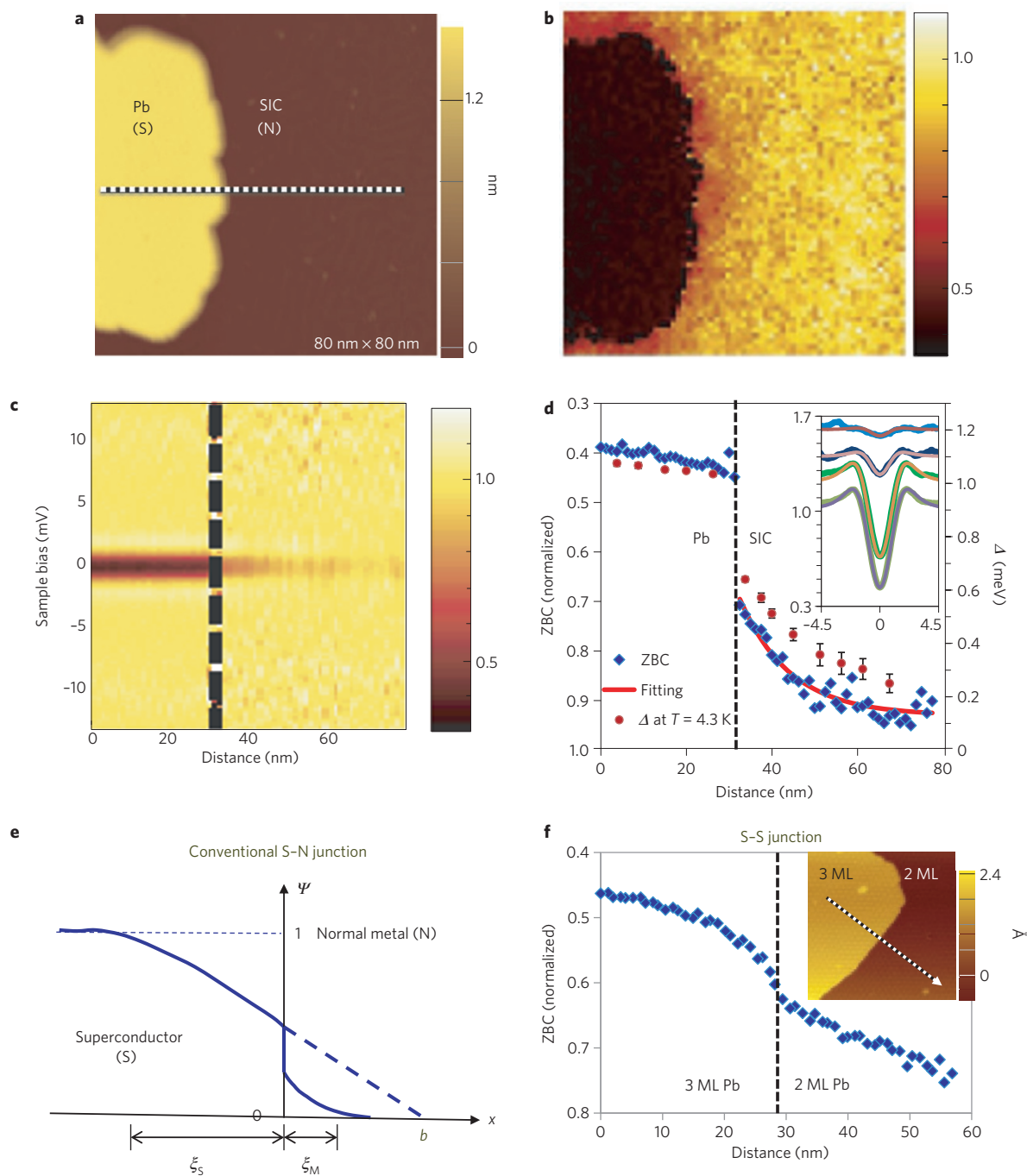


Figure 2 | Proximity effects on a simple junction of SIC surface (N)-Pb island (S). **a**, STM topography image showing a junction of SIC surface-Pb island (sample bias $V_s = 0.3$ V, tunnelling current $I_t = 10$ pA). **b**, Normalized ZBC image measured at 4.3 K for the same area of **a**. **c**, The spatial dependence of superconducting gap spectra at 4.3 K measured along the dashed line in **a**. **d**, ZBC profile and the fitted superconducting gap profile extracted from **c** showing the variation of superconducting order across the physical boundary. (An exponential function of $-3.78e^{-x/11.7} + 0.93$ is used for the fitting.) Note that the ZBC profile is plotted with the high value (small gap) pointing down to be qualitatively consistent with the profile of the gap value (Δ). The error bars in Δ represent the minimum and maximum values measured for each data point. The inset shows fitting examples of the normalized dI/dV spectra with the BCS density of state (each spectrum is offset successively for clarity). **e**, Schematic profile describing the qualitative behaviour of the order parameter/pair correlations across a conventional S-N junction. **f**, The ZBC profile across a superconductor-superconductor (S-S) junction formed by a 3 ML Pb island connected to a larger 2 ML Pb island (the inset shows the corresponding 50 nm \times 50 nm STM image).

We note that in a recent investigation of a 1D S-N-S junction comprised of a metallic nanowire with superconductor contacts at two ends, minigaps existed in the normal metal nanowire over an extended region¹. Moreover, the result is quantitatively consistent with the solutions of the nonlinear Usadel equation⁸. In this sense, our observation of a superconducting gap existing over an

extended length scale in the 2D S-N-S double junctions shares some similarities. In fact if a 2D S-N-S junction is infinitely long along the parallel direction, it is theoretically the same as a 1D S-N-S junction. However, the 2D system exhibits profound manifestations of geometric influence on the proximity effect that do not exist in a 1D system. For example, as shown in Fig. 1c, markedly different

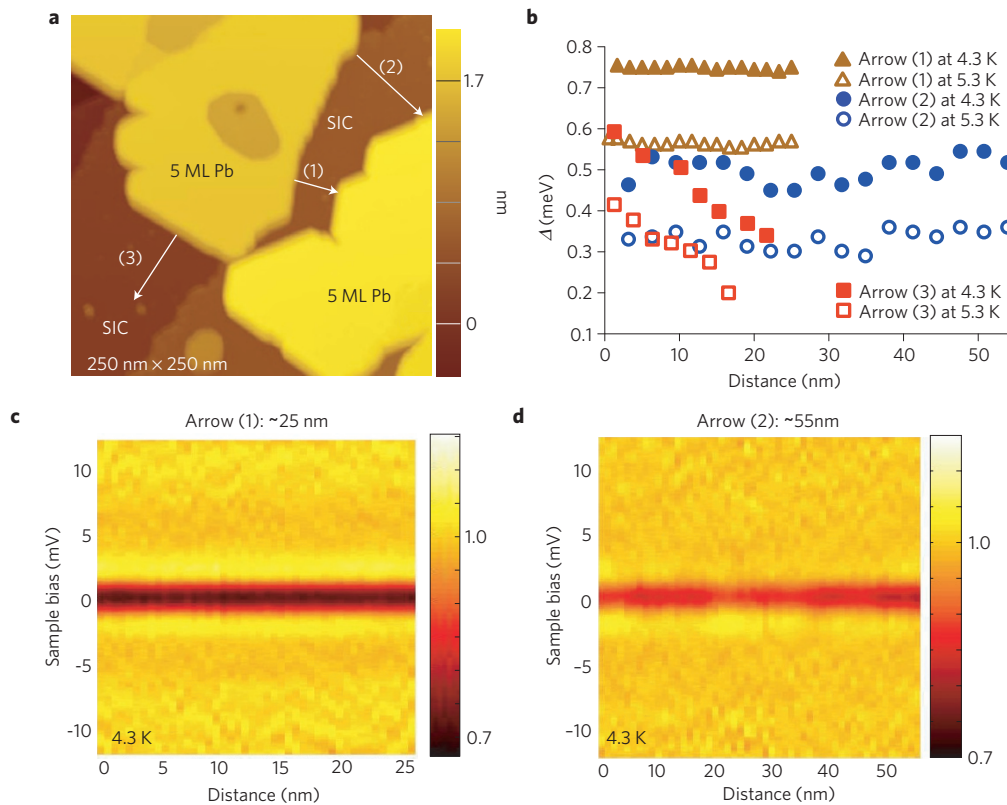


Figure 3 | Proximity effects on various confined geometries of Pb island (S)-SIC surface (N)-Pb island (S). **a**, STM topography image of two 5 ML Pb islands that provide confined geometry for the SIC area marked as arrow (1) and (2) (sample bias $V_s = 0.3$ V, tunnelling current $I_t = 10$ pA). **b**, The extracted energy gap Δ values as a function of distance along the arrows in **a**. The length of arrows (1), (2) and (3) is around 25 nm, 55 nm and 40 nm, respectively. **c,d**, The spatial dependence of superconducting gap spectra at 4.3 K measured along arrow (1) (**c**) and arrow (2) (**d**).

behaviours are observed for regions α and γ . Both are open S-N junctions, but in region α , the superconducting island has a positive curvature (resulting in a very short proximity length), whereas in region γ , there is a negative cusp in the superconductor island that results in a much longer proximity length.

The geometric manifestation of the proximity effect is investigated further by studying another junction geometry—the surrounded junction where a hole (or a few holes) exposes the SIC region in a Pb island (Fig. 4a). In such ‘surrounded’ junctions, we observe an even more robust superconducting gap in the SIC for holes with an effective diameter of up to 60 nm. Interestingly, the ratio between the gap value measured in the hole and that measured in the surrounding Pb island remains relatively constant over a wide range of temperatures. Fitting Δ versus T with the BCS model, one finds that the data at different spatial locations (Pb island, different holes) converge to the same T_C owing to this constant gap ratio. This is a direct consequence of the fact that the superconducting gap observed in the SIC is completely induced by the proximity effect. Thus, even though the strengths of the induced superconducting gaps in different holes are different, they all converge to the same T_C .

We have further carried out a systematic investigation of how the strength of the induced superconducting gap varies with respect to the size of the normal region in both the S-N-S double-sided junction and the surrounded junction. In Fig. 4b, we plot the ratio between the gaps measured on the surrounding Pb islands and those at the centre of the SIC structures. The variable, d , represents either the effective hole diameter of the surrounded junction or the size of the normal region in the S-N-S two-sided junction. As one expects, the larger the size of the normal region, the weaker the induced gap. Moreover, in the surrounded junction, the strength of the induced gap is much higher than that of the S-N-S two-sided junction.

To quantitatively account for such intriguing manifestations of junction geometry on the proximity effect, we have carried out theoretical calculations to solve the Usadel equation for two different models: a quasi-1D model for a S-N-S two-sided junction where the dimension parallel to the junction is extended to infinity; and a 2D model for a surrounded junction with a circular symmetry (Fig. 4b). These two models represent two idealized junction geometries for calculation simplicity. However, they should capture the underlying physics behind the observed phenomena, in particular the different scaling behaviour. The most relevant parameter in the calculation is the ratio between the size of the normal metal and the coherent length, d/ξ . The theoretical calculation indeed reveals different scaling behaviour between the two models. The results for two different models are plotted as dashed curves in Fig. 4b using a coherent length of 24 nm. The comparison between the theoretical simulations and the experimental results shows a good quantitative agreement, particularly for the surrounded junction. For the quasi-1D model, deviation is observed for $d < 40$ nm. This deviation is anticipated because the actual S-N-S junctions in the experiment all have finite lateral length L . Most measurements in our experiment for smaller d values are accompanied with shorter lateral lengths. In comparison the idealized circular junction provides a better approximation for the surrounded junction, thus yielding better quantitative agreement.

Although we have carried out calculations for only these two idealized junction geometries, the quantitative agreement with the experimental result allows us to draw general conclusions on the mechanism behind the intriguing manifestation of junction geometry on the proximity effect. At a fundamental level, the proximity effect at a S-N junction is due to Andreev reflection.

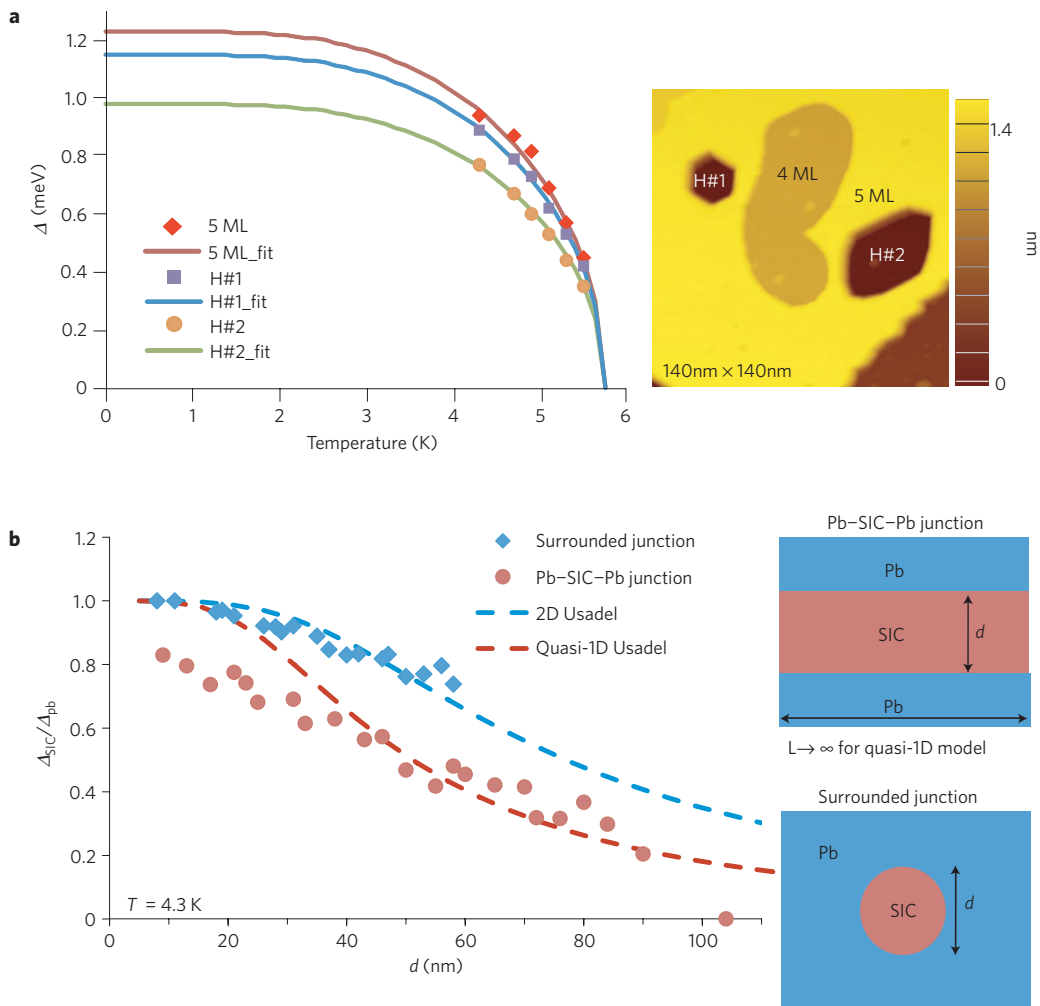


Figure 4 | Geometric influences on proximity effects. **a**, The superconducting energy gap as a function of temperature, $\Delta(T)$, measured at different regions of the corresponding STM image in the inset. The STM image shows an island containing 5 ML and 4 ML regions as well as two holes (H#1 and H#2) in the 5 ML region exposing the SIC wetting layer. Also shown are the three fitting curves for these $\Delta(T)$ using a BCS gap equation. Note that despite a different gap value, all three curves fall into the same T_C of $\sim 5.7 \pm 0.1$ K. In the inset, the hole sizes of H#1 and H#2 are around 19 nm and 35 nm, respectively. **b**, The gap ratio of Δ_{SiC} to Δ_{Pb} at 4.3 K was measured as a function of the junction distance, d , for 1D and 2D confined heterojunctions described by schematics to the right-hand side.

For a quasi-1D S–N–S double-sided junction, Andreev reflections occur at both interfaces multiple times, which would lead to an enhanced proximity effect. It should be mentioned that there exists a wealth of literature discussing the difference between S–N interfaces and S–N–S junctions. Some have discussed the role of multiple Andreev reflections to account for the coherent charge transport across a S–N–S junction^{23–26}. The real-space STM/S investigation here brings out the direct contrast between S–N and S–N–S junctions. In addition, it allows us to gain new insight into how the 2D junction geometry profoundly impacts the proximity effect. For example, when there is a negative curvature at the S–N interface (viewed from the superconductor side), Andreev reflections seem to converge, leading to an apparently longer proximity length (region γ in Fig. 1c) or diverge for a positive curvature (region α). For a surrounded junction, the Andreev reflection converges from all sides, thus leading to a much stronger proximity effect. Although qualitative in nature, this argument accounts for all of our observations: enhanced proximity effects for S–N–S double-sided junctions, even more enhancement for surrounded junctions and the influence of the curvature of the junction interface. This argument is further substantiated by the quantitative agreement between the theoretical calculations and

the experimental results in two different junction geometries: a quasi-1D S–N–S double junction and a 2D circular junction.

Methods

Sample preparation. The experiments were conducted in a home-built low-temperature STM system with an *in situ* sample preparation chamber. A Pb–Si reconstructed surface of the SIC phase was prepared by deposition of ~ 1 ML of Pb onto the Si(111) 7×7 surface at room temperature, followed by sample annealing at 400–450 °C for 4 min to form the surface template (see Supplementary Fig. S1). To get 2D islands, Pb was deposited on the template at ~ 200 K with a deposition rate of 0.5 ML per minute. Before transferring *in situ* to the low-temperature STM stage, the sample was annealed briefly at ~ 200 K for 3 min. Pb 2D islands on top of SIC surfaces with various shapes and thicknesses make an ideal system to investigate the influence of geometry on proximity effects.

STS. Electrochemically etched tungsten tips treated with *in situ* electron-beam cleaning were used for all measurements. All differential conductance spectra were taken with the same tunnelling parameter with the junction stabilized at $V_s = 20$ mV and $I_t = 30$ pA tunnelling current. To eliminate possible piezo creeping and thermal drift, the piezo scanner (an STM tip) was stabilized at the required area for more than 8 h at 4.3 K before each ZBC measurement. The same tunnelling parameter (stabilized at 17 mV with 20 pA tunnelling current) was used for all ZBC measurement. ZBC images were normalized by using a high-order (in this case, fifth order) polynomial to fit the spectra outside the gap region to represent the normal DOS. This normalization procedure works quite well for a general shape even when

the normal DOS contains a dip or peak. More details of the normalization method are well described in our previous publication¹⁹.

Received 19 September 2011; accepted 9 March 2012;
published online 15 April 2012; corrected after print 16 March 2015

References

- Gueron, S. *et al.* Superconducting proximity effect probed on a mesoscopic length scale. *Phys. Rev. Lett.* **77**, 3025–3028 (1996).
- Belzig, W. *et al.* Quasiclassical Green's function approach to mesoscopic superconductivity. *Superlatt. Microstr.* **25**, 1251–1288 (1999).
- Pannetier, B. & Courtois, H. Andreev reflection and proximity effect. *J. Low Temp. Phys.* **118**, 599–615 (2000).
- Dirks, Travis *et al.* Transport through Andreev bound states in a graphene quantum dot. *Nature Phys.* **7**, 386–390 (2011).
- Pillet, J. D. *et al.* Andreev bound states in supercurrent-carrying carbon nanotubes revealed. *Nature Phys.* **6**, 965–969 (2010).
- Wang, J. *et al.* Proximity-induced superconductivity in nanowires: Minigap state and differential magnetoresistance oscillations. *Phys. Rev. Lett.* **102**, 247003 (2009).
- le Sueur, H. *et al.* Phase controlled superconducting proximity effect probed by tunnelling spectroscopy. *Phys. Rev. Lett.* **100**, 197002 (2008).
- Usadel, K. D. The diffusion approximation for superconducting alloys. *Phys. Rev. Lett.* **25**, 507–509 (1970).
- Nazarov, Yu. V. Novel circuit theory of Andreev reflection. *Superlatt. Microstr.* **25**, 1221–1231 (1999).
- Kamenev, A. & Levchenko, A. Keldysh technique and non-linear sigma model: Basic principles and applications. *Adv. Phys.* **58**, 197–319 (2009).
- Belzig, W., Bruder, C. & Schn, G. Local density of states in a dirty normal metal connected to a superconductor. *Phys. Rev. B* **54**, 9443–9448 (1996).
- Cuevas, J. C. *et al.* Proximity effect and multiple Andreev reflections in diffusive superconductor normal-metal superconductor junctions. *Phys. Rev. B* **73**, 184505 (2006).
- Ganz, E. *et al.* Growth and morphology of Pb on Si(111). *Surf. Sci.* **257**, 259–273 (1991).
- Seehofer, L., Falkenberg, G., Daboul, D. & Johnson, R. L. Structural study of the close-packed two-dimensional phases of Pb on Ge(111) and Si(111). *Phys. Rev. B* **51**, 13503–13515 (1995).
- Hupalo, M. *et al.* Atomic models, domain-wall arrangement, and electronic structure of the dense Pb/Si(111)- $\sqrt{3} \times \sqrt{3}$ phase. *Phys. Rev. B* **66**, 161410 (2002).
- Qin, S. Y., Kim, J., Niu, Q. & Shih, C. K. Superconductivity at the two-dimensional limit. *Science* **324**, 1314–1317 (2009).
- Zhang, T. *et al.* Superconductivity in one-atomic-layer metal films grown on Si(111). *Nature Phys.* **6**, 104–108 (2010).
- Eom, D., Qin, S., Chou, M. Y. & Shih, C. K. Persistent superconductivity in ultrathin Pb films: A scanning tunnelling spectroscopy study. *Phys. Rev. Lett.* **96**, 027005 (2006).
- Kim, J. *et al.* Universal quenching of the superconducting state of two-dimensional nanosize Pb-island structures. *Phys. Rev. B* **84**, 014517 (2011).
- Bardeen, J., Cooper, L. N. & Schrieffer, J. R. Theory of superconductivity. *Phys. Rev.* **108**, 1175–1204 (1957).
- Tinkham, M. *Introduction to Superconductivity* 2nd edn (Dover, 1996).
- Ozer, M. M., Thompson, J. R. & Weitering, H. H. Hard superconductivity of a soft metal in the quantum regime. *Nature Phys.* **2**, 173–176 (2006).
- Dubos, P., Courtois, H., Buisson, O. & Pannetier, B. Coherent low-energy charge transport in a diffusive S–N–S junction. *Phys. Rev. Lett.* **87**, 206801 (2001).
- Ohta, H. & Matsui, T. Nanometer SNS junctions as quantum-well devices. *IEEE Trans. Appl. Supercond.* **7**, 2814–2817 (1997).
- Sipr, O. & Gyorffy, B. L. Interpretation of bound states in inhomogeneous superconductors: The role of Andreev reflection. *J. Phys. Condens. Matter* **8**, 169–191 (1996).
- Zhou, F., Charlat, P., Spivak, B. & Pannetier, B. Density of states in superconductor–normal metal–superconductor junctions. *J. Low Temp. Phys.* **110**, 841–850 (1998).

Acknowledgements

We are grateful to L. Glazman and A. Kamenev for discussions. This work was supported by DMR-0906025, Welch Foundation F-1672, ARO W911NF-09-1-0527 and NSF DMR-0955778.

Author contributions

J.K. and C-K.S. designed and coordinated the experiments; J.K. and H.N. carried out the experiments; V.C., G.A.F. and A.H.M. performed the theoretical calculations; J.K., V.C., G.A.F., H.N., A.H.M. and C-K.S. analysed the data; J.K., G.A.F. and C-K.S. wrote the paper.

Additional information

The authors declare no competing financial interests. Supplementary information accompanies this paper on www.nature.com/naturephysics. Reprints and permissions information is available online at www.nature.com/reprints. Correspondence and requests for materials should be addressed to C-K.S.

Visualization of geometric influences on proximity effects in heterogeneous superconductor thin films

Jungdae Kim, Victor Chua, Gregory A. Fiete, Hyungdo Nam, Allan H. MacDonald and Chih-Kang Shih

Nature Physics **8**, 464–469 (2012); published online 15 April 2012; corrected after print 16 March 2015.

In the version of this Letter originally published the article number in reference 6 contained a typographical error and should have read 247003. This has now been corrected in the online versions of the Letter.